# IRAN : INTERFEROMETRIC REMAPPED ARRAY NULLING

E. Aristidi, F. Vakili, A. Schutz, H. Lantéri, L. Abe, A. Belu, P. M. Gori, O. Lardière, B. Lopez, J. L. Menut, et al.

*Title : will be set by the publisher*
*Editors : will be set by the publisher*
*EAS Publications Series, Vol. ?, 2005*

# IRAN : INTERFEROMETRIC REMAPPED ARRAY NULLING

Aristidi E.[1], Vakili F.[1], Schutz A.[1], Lanteri H.[1], Abe L.[1], Belu A.[1], Gori P.M.[1], Lardière O.[2], Lopez B.[3], Menut J.L.[3] and Patru F.[3]

**Abstract.** IRAN is a method of beam-combination in the hypertelescope imaging technique recently introduced by Labeyrie in optical interferometry. We propose to observe the interferometric image in the pupil plane, performing multi-axial pupil plane interferometry. Imaging is performed in a combined pupil-plane where the point-source intensity distribution (PSID) tends towards a pseudo Airy disc for a sufficiently large number of telescopes. The image is concentrated into the limited support of the output pupil of the individual telescopes, in which the object-image convolution relation is conserved. Specific deconvolution algorithms have been developped for IRAN hypertelescope imagery, based upon Lucy-like iterative techniques. We show that the classical (image plane) and IRAN (pupil plane) hypertelescope imaging techniques are equivalent if one uses optical fibers for beam transportation. An application to the VLT/VIDA concept is presented.

## 1 Introduction (retravailler la fin)

The concept of densified pupil-hypertelescope introduced by Labeyrie (1996) is a generalization of the classical Michelson periscopic set-up for stellar interferometry (Michelson, 1920). The principle is to increase the relative pupil size of individual telescopes (output pupil diameters normalized to the baselines) composing the interferometer, to fill up the disc of the equivalent single dish telescope. This non linear process modifies the classical object-image convolution relation for extended sources larger than the Airy discs of individual telescopes. Thus the non-aberrated imaging field of view can dramatically decrease with increasing so-called densification factor $\gamma$ (Gillet et al., 2003).

We recently proposed a multiaxial pupil-plane imaging technique (Vakili et al., 2004) which is equivalent to Labeyrie's hypertelescope technique with the extra

[1] LUAN, Université de Nice – Parc Valrose – 06108 Nice Cedex 2, France
[2] Observatoire de Haute Provence, France
[3] Observatoire de la Cote d'Azur, France


DOI: (will be inserted later)

bonus of conserving the convolution relation over a field limited to the superimposed pupilla of the primary telescopes. Images this way formed in the pupil plane are similar to what can be expected at the focus of the giant equivalent telescope, excepted that the field is spatially limited by the geometrical image of the telescope pupils. This property is interesting in particular for exoplanet (ExPN) observations: compared to coaxial Bracewell nulling interferometry (Bracewell, 1978), our concept presents the advantage of separating the ExPN energy from the zodiacal emission of its parent star. The paper is organised as follows. In section 2 we give the general formalism for object-image relation. In section **??** we focus on stellar companions detection and propose an apodisation technique for reducing the main star PSID secondary peaks. In section 3 we propose a deconvolution method for extended objects. Finally, in section 4 we discuss the combination of the interferometer with a AIC-type nuller (Gay & Rabbia, 1996) to perform high-dynamic exoplanet detection.

## 2 Principle of IRAN

Labeyrie's hypertelescope concept (Labeyrie, 1996) is based on densifying the output pupil of an interferometric array by conserving the primary telescope orientations respective to each other to form the equivalent of a single dish telescope with a continuous surface. This is obtained for instance by re-imaging the output pupils on a pyramidal beam combiner (Gillet et al., 2003). The resulting diffraction pattern is formed by coherent addition of tilted Airy discs of individual telescopes. It exhibits a complicated fringe modulated image which tends to the Airy disc of the pseudo-densified aperture, thus resembling to a monolithic giant dish Airy pattern. In the IRAN concept beam-combination is simply obtained by forming tilted output pupils on the top of each other and record their interference on a 2D detector. The tilt given to each pupil is proportionnal to the position of the telescopes on the ground (conformal geometry). As discussed hereafter, this can be achieved by forming an intermediate image plane and using a lens to form the interferometric pupil plane. Or by tilting the collimated beams from each telescope so that they intersect and use lenses to form a geometric image of the pupil at the intersection.

### *2.1 Technical implementation*

To better understand the operating principle of IRAN it is useful to recall Michelson optical set-up for stellar interferometry (Fig. 1, left). In our two-telescopes example, collimated beams are transported to the interferometric lab where output pupils are formed, an a relay lens produces the interferometric image. The fringe modulation does not depend on the spacing between the input telescope pupil size but on the output pupils as seen from the focal superimposed Airy patterns. In the Michelson set-up the basic convolution relation between the point spread function and the object intensity distribution on the sky is lost (excepted if the object is small compared to the diffraction limit of individual telescopes)

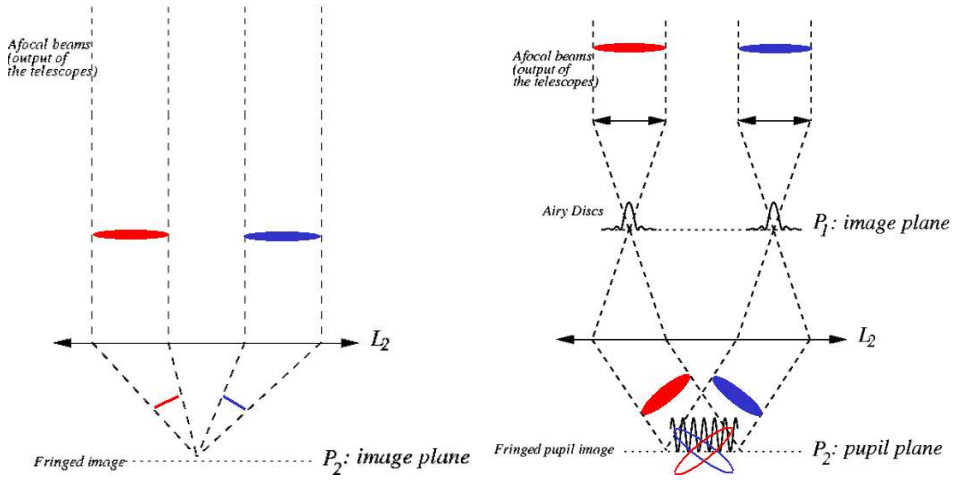


**Fig. 1.** Principle of the Michelson (left) and IRAN (right) beam-combiner. In the Michelson setup, collimated beams coming from the telescopes are focused by a common lens $L_2$ in the image plane, producing a fringed Airy disc. Output pupil plane is schematised by the two ellipses. In the IRAN setup, a lens focuses every collimated beam into an Airy disc in the intermediate image plane $P_1$. The same common lens $L_2$ produces a fringed pupil image in the pupil plane $P_2$. The function descriving the intensity of the fringe pattern is the same in both cases.

making image reconstruction from the measure of the complex visibility function mandatory. The fringe intensity pattern is modulated by the Airy envelope.

The Michelson set-up can be further modified (Chelli & Mariotti, 1986) to form the Airy discs of individual telescopes at an intermediate image plane, then a relay lens which would form two superimposed and cosine-modulated output pupils where the fringe period depends on the Airy disc pattern distance as seen from the two superimposed pupils (Fig. 1, right). We name IRAN this set-up. Now if much more than two beams were remapped from a large number of input mirror segments the different period and orientation of the resulting cosine fringe modulations will produce a central bright spot at the center of the conjugate stacked pupil for an on-axis star.

Two beam-combination schemes could be envisaged in this case: a classical bulky optical pyramidal shape mirror (Rousselet-Perraut et al., 1997) which generalizes the above set-up versus a fiber optics (F.O.) beam combiner (Mariotti et al., 1996) with the bonus of modal filtering and an expected simplified beam-combiner. In the case of F.O. combination, the field of view would be limited to the Airy angular size of individual telescopes.

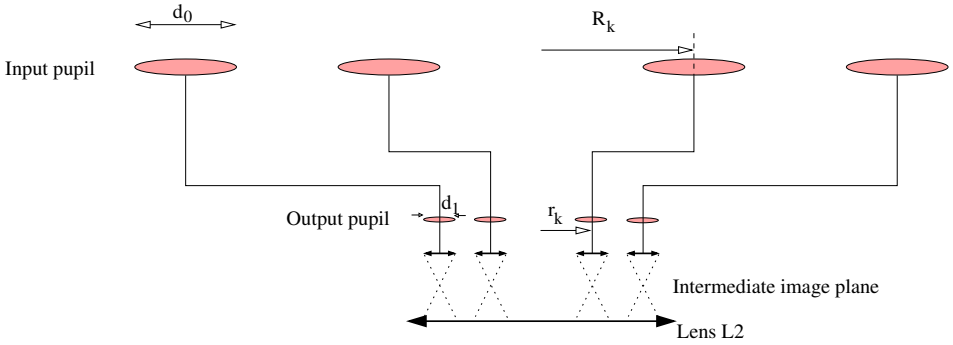


**Fig. 2.** Geometry of the interferometer. The input-to-output reduction factor of the distances between the telescopes is $\gamma = R_k/r_k$. The same factor for the individual pupils diameters is $\gamma_d = d_0/d_1$

### *2.2 On-axis point-source intensity distribution*

The IRAN formalism has been discussed in previous papers (Vakili et al., 2004, Aristidi et al., 2004), we will recall here the main results and compare them with the Michelson set-up formalism. Let $\vec{R}_k$ the positions of the $N$ telescopes on the ground, $P$ the input pupil function of the telescopes. These telescopes are supposed identical, with diameter $d_0$. We suppose that the incoming light is monochromatic with wavelength $\lambda$. Let $\vec{r}_k$ be the position of the center of the optical beams after reconfiguration. We suppose that the geometry of the output pupil is conserved and introduce the factor $\gamma$ defined as $\vec{R}_k = \gamma\vec{r}_k$. We denote as $d_1$ and $f_1$ the diameter and focal of the lenses making the adjacent Airy discs in the intermediate focal plane $P_1$. We denote as $f$ the focal length of the lens $L_2$ producing the interferometric image. The whole geometry is illustrated in Fig 2.

The intensity distribution of the output pupil expresses as

$$P_o(\vec{r}) = p(\vec{r}) * \sum_{k=1}^{N} \delta(\vec{r} - \vec{r}_k) \tag{2.1}$$

where $p(\vec{r}) = P(\gamma_d\vec{r})$ is the pupil function of each telescope after beam transportation and $\gamma_d$ the input-to-output reduction factor of the individual pupils (we speak about pupil densification if $\gamma_d \neq \gamma$). In the standart Michelson setup, the on-axis PSID is then

$$I_M(\vec{r}) = \left|\hat{p}\left(\frac{\vec{r}}{\lambda f}\right)\right|^2 \cdot \left|\sum_{k=1}^{N} \exp -\frac{2i\pi}{\lambda f}(\vec{r}.\vec{r}_k)\right|^2 \tag{2.2}$$

The IRAN PSID is (Vakili et al., 2004)

$$I(\vec{r}) = \left|p\left(-\frac{\vec{r}f_1}{f}\right)\right|^2 \cdot \left|\sum_{k=1}^{N} \exp -\frac{2i\pi}{\lambda f}(\vec{r}.\vec{r}_k)\right|^2 \tag{2.3}$$

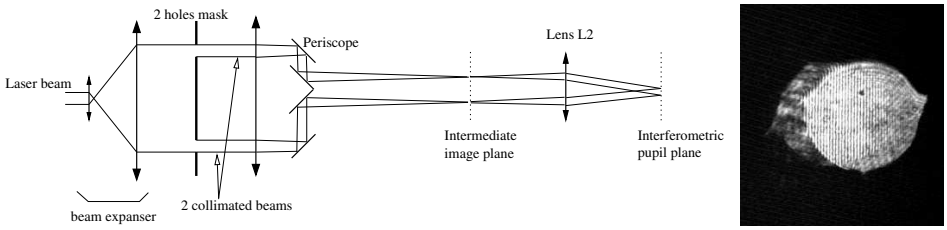


**Fig. 3.** Optical layout of the IRAN 2-beams laboratory experiment (left), and recorded interferometric image (fringed pupil) on the right.

These two expressions are the product of two terms: (i) an identical *interference function* $I_0(\vec{r}) = \left|\sum_{k=1}^{N} \exp -\frac{2i\pi}{\lambda f}(\vec{r}.\vec{r}_k)\right|^2$ depending only on the position of the centers of the individual output pupils, and (ii) an enveloppe function that changes with the setup: the pupil function of individual telescopes in IRAN setup, or its Fourier transform in Michelson setup. This enveloppe constitutes the physical limit of the field of view (FOV) of the interferometer.

**Laboratory experiment**

To validate the concept, we made a simple laboratory experiment for a 2-pupil interferometer using laser light. The optical scheme is presented in Fig. 3: a laser beam is enlarged by a 2-lens beam expanser, producing a collimated beam. Then, with a 2-holes mask simulating the hypertelescope pupil, we realise 2 parallel beams. A convergent lens and a periscope placed into each beam produces two adjacent Airy discs in an intermediate image plane. Another common lens (above mentionned $L_2$) creates the interferometric image. Here it is simply a cosine-modulated pupil. The result of this experiment is shown in Fig. 3. We obtained two superposed pupils (not completely because of alignement problems) showing interference fringes.

**Case of a fiber optics beam combiner**

We consider the case where the light incoming from the telescopes is injected into monomode optical fibers, then transported to the interferometric lab. If one makes the classical assumption that the wavefront at the exit of the fiber is flat with a Gaussian shape, then the above formalism is unchanged. The only difference being in the function $p(\vec{r})$ describing the outut pupil function of the individual telescopes, which is now a Gaussian (in fact there is no more pupil plane in this case, and $p(\vec{r})$ is simply the complex amplitude of the wave for each beam). Therefore, in IRAN setup *as well as in Michelson setup*, the intensity distribution of the interferometric image is a fringe modulated Gaussian (Fig. 4).

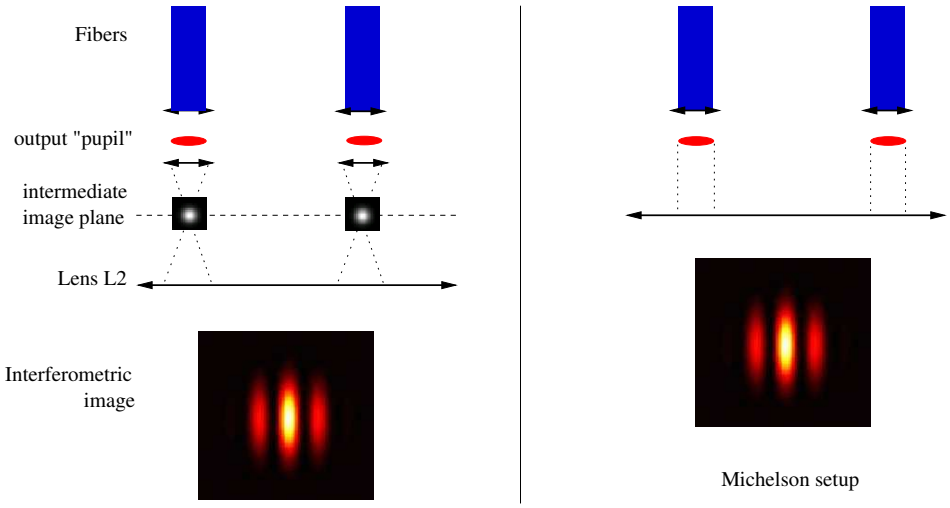


**Fig. 4.** Comparison of IRAN (left) and Michelson (right) setups for a fiber optics beam transport.

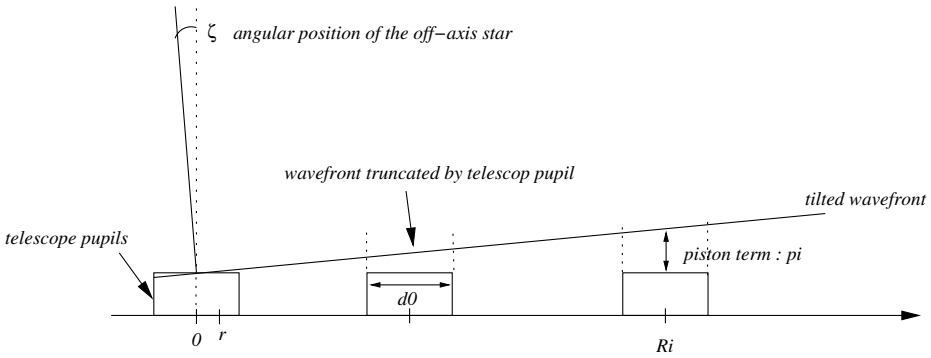


**Fig. 5.** Simulated observation of an off-axis point-source at a distance $\zeta$ from the center of the field of view. On this one-dimensionnal configuration, each telescope is at a position $R_i$. The corresponding complex amplitude on each pupil is the product of a piston term $\exp 2i\pi\zeta R_i/\lambda$ by a tilt term $\exp 2i\pi\zeta r/\lambda$, $r$ being the coordinate inside the pupil function.

### *2.3 The response for an off-axis point-source*

We observe an off-axis point source of intensity $O_0$ in the direction given by the vector $\vec{\zeta} = (\alpha, \delta)$ where $\alpha$ (resp. $\delta$) is the offset in right ascension (resp. declination, see fig. 5 for illustration). The incident flat wavefront is tilted with an angle $\vec{\zeta}$. This wavefront is sampled by the $N$-apertures pupil. For each sub-pupil, the products of two terms appear in the complex amplitude on the pupil: a piston

term depending on the telescopes position

$$p_i = \exp \frac{2i\pi\vec{\zeta}.\vec{R}_i}{\lambda} \tag{2.4}$$

and a tilt term

$$t = \exp \frac{2i\pi\vec{\zeta}.\vec{r}}{\lambda} \tag{2.5}$$

where $\vec{r}$ is a position on the single telescope pupil. The piston term will be conserved in the output pupil plane, regardless of the beam transort system (bulky optics or fibers). The behaviour of the tilt term depends of the optical configuration. In case of bulky optics, the slope of the tilt will be multiplied by the compression factor $\gamma_d$; the tilt in the output individual telescope pupils expresses as

$$t' = \exp \frac{2i\pi\vec{\zeta}.\gamma_d\vec{r}}{\lambda} \tag{2.6}$$

. In case of fiber optics beam transport, the tilt term simply vanishes, if the tilt is small compared to the numerical aperture of the fiber, because of spatial filtering.

The piston term is responsible for a motion of the interference fringes in the focal plane, in both Michelson and IRAN setups. It has the same effect that putting a parralel glass plate onto one hole of a Fizeau 2-holes interferometer. Note that the piston term has no effect on the enveloppe of the fringes.

In IRAN setup, the tilt term is responsible for an identical motion of all subimages in the intermediate image plane $P_1$. It has no effect on the interferometric image intensity distribution (it will multiply the enveloppe of the fringes by a complex term which vanishes when taking the square modulus). Therefore the enveloppe of the fringes does not move for an off-axis point source.

In Michelson setup, in the case of bulky optics, the tilt term is responsible for a motion of the enveloppe of the fringes (Labeyrie, 1996). If $\gamma_d \neq \gamma$, the motion speed of the fringes and the enveloppe are not the same.

In Michelson setup with a fiber optics beam transportation, the tilt vanishes and the enveloppe no longer moves away of the optical axis. in that case the image formation is similar to IRAN: a stable enveloppe in which the fringe system moves.

Vakili et al. (2004) derived the intensity distribution of the off-axis PSID of the interferometric image in IRAN setup:

$$I_2(\vec{r}) = O_0\Pi(\vec{r}) \; . \; I_0\left(\vec{r} - \gamma f\vec{\zeta}\right) \tag{2.7}$$

Where $\Pi(\vec{r}) = \left|p\left(-\vec{r}\frac{f_1}{f}\right)\right|^2$ is the enveloppe of the fringes. As for the on-axis case, this term is a geometrical limitation of the field in the pupil plane. Within this field, the function $I_2(\vec{r})$ satisfies the property of translation invariance. Therefore, as written hereafter, a pseudo-convolution relation will exist between the source and its image. Note that this is valid also in Michelson fiber optics setup; the difference being the function $\Pi(\vec{r})$.

This is a fundamental difference with the bulky optics Labeyrie/Michelson pupil-densified concept, where the fringes in the interferometric plane are shaped by an enveloppe which shifts when the star moves away from the optical axis. In this case both structures (fringes and enveloppe) moves at a different speed. No convolution relation exists, unless the size of the object is small compared to the individual Airy discs of the telescope (in that case the enveloppe motion is neglectible and the two recombinations are equivalent).

### *2.4 Object-image relation*

We now consider the general case of on object of brightness distribution $O(\vec{\zeta})$. The object-image relation writes as the pseudo-convolution (Vakili et al., 2004):

$$I_2(\vec{r}) = \left(\frac{1}{\gamma f}\right)^2 \Pi(\vec{r}) \ \left[I_0(\vec{r}) * 0 \left(\frac{\vec{r}}{\gamma f}\right)\right] \tag{2.8}$$

Inside the boundaries delimited by the pupil function $|P(\vec{r})|^2$, we find the classical convolution relation between the PSID and the object scaled by the factor $\gamma f$. This factor allows to convert a position $x$ in meters in the focal plane into an angle $\zeta = \frac{x}{\gamma f}$ in radian on the sky.

The object-image convolution relation of Eq. 2.8 is an interesting property for imagery at the interferometer resolution. In the simple case of a double star, the focal image is the sum of two PSIDs at a distance corresponding to the star and its companion separation times the magnification factor and weighted by their intensity ratio. Fig. 6 presents a simulation of an interferometric image obtained with a 39 apertures hypertelescope pupil with bulky optics, in IRAN and Michelson setups, for an on-axis and off-axis point source, and for a double star. The pupil function (drawn on the left on the figure) is composed of 39 1 m diameter telescopes observing at $\lambda = 10\mu$m. The telescopes are spread over 3 rings of diameters 120 m, 240 m and 380 m. (a) and (d) are the on-axis PSID for IRAN and Michelson setups. The interference funnction in that case is very close to an Airy disc near the center of the figure, then some speckle-like noise appears due to the incomplete coverage of the equivalent giant single dish aperture. On the off-axis PSID (figures (b) and (e)) the interference function has moved inside the enveloppe. One can see that in the Michelson case, the space-invariance is not respected (the interference pattern is no more symmetric). Figures (c) and (f) are a double star image with separation 50 mas and 1 magnitude difference.

## 3 Deconvolution

A deconvolution algorithm based on likelihood maximisation has been implemented to invert the object image relation (eq. 2.8) and reconstruct the observed object (denoted by $x$ in this paragraph) from its image ($y$) and an estimation of the PSID (made for example on a nearby reference star). The PSID is a truncated (or partially hidden) image of the PSF $h$ ($h$ is the function $I_0$ in eq. 2.8).

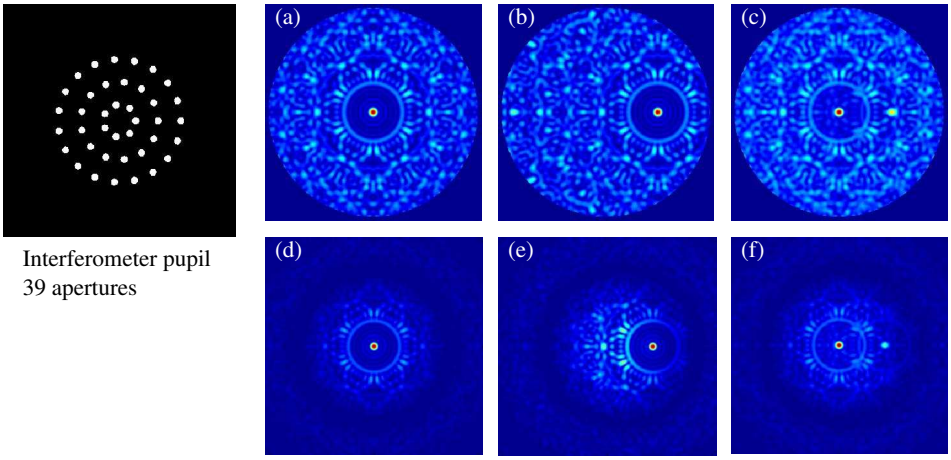


**Fig. 6.** Simulation of interferometric images for a 39 telescopes pupil. Left: pupil function. (a) IRAN on-axis PSID. (b) IRAN off-axis PSID. (c) IRAN double star image. (d) Michelson on-axis PSID. (e) Michelson off-axis PSID. (f) Michelson double star image.

The signal restoration problem consists in the reconstruction of the best estimate $x$ from the knowledge of a blurred signal $y$ contaminated by noise. In our case we consider a photon noise process. The transformation suffered by $x$ is described by a convolution which can be written as:

$$\tilde{y}(r,s) = B \ \times \ [h(r,s) * x(r,s)] \tag{3.1}$$

with $\iint h(r,s)drds = 1$ (PSF is supposed to be normalised). where $\tilde{y}(r,s)$ is the noiseless blurred signal, $h$ the PSF, $x$ the object and $B$ the circular mask (pupil function). It is important to note that part of the signal is hidden after the convolution. For example if the object is an unresolved star we only have the PSID estimate $B \times h$ and the complete PSF $h$ cannot be obtained. This is one of the main difficulties of this inversion problem; in particular classical algorithms such as Richardson-Lucy do not apply to this case.

For a photon noise process, the intensity in the pixel $i$ is a random variable which follows a Poisson law with mean $B_i \times [h * x]_i$. The likelihood expresses as:

$$L(x) = p(y|x) = \prod_i \frac{(B_i \times [h * x]_i)^{y_i}}{y_i!} \ \exp -(B_i \times [h * x]_i) \tag{3.2}$$

The deconvolution algorithm is deduced from the split gradient method SGM (Lanteri et al., 2002). The application to our problem gives the multiplicative iterative algorithm:

$$\hat{x}_i^{(k+1)} = m_i + (x_i^{(k)} - m_i) \left[ \frac{h(-r,-s) * \frac{y}{h(r,s)*x^{(k)}} + \epsilon}{h(-r,-s) * B + \epsilon} \right]_i \tag{3.3}$$

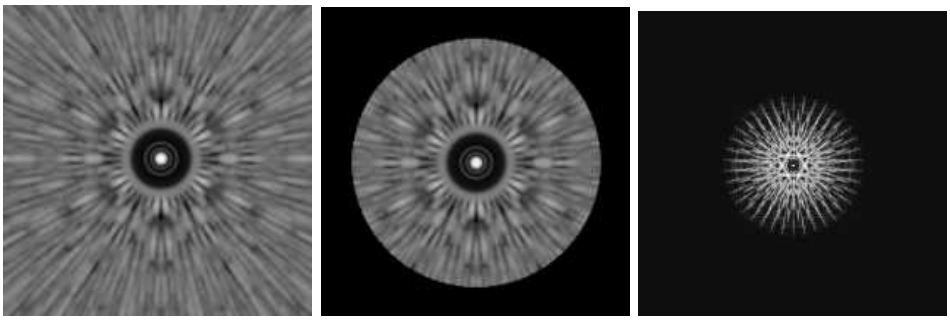

**Fig. 7.** Polychromatic PSF simulation for a 39 telescopes interferometer. Left: the complete PSF. Middle: the central part of the PSF, that can be estimated on a reference star. Right: The Fourier transform of the PSF showing limited support.

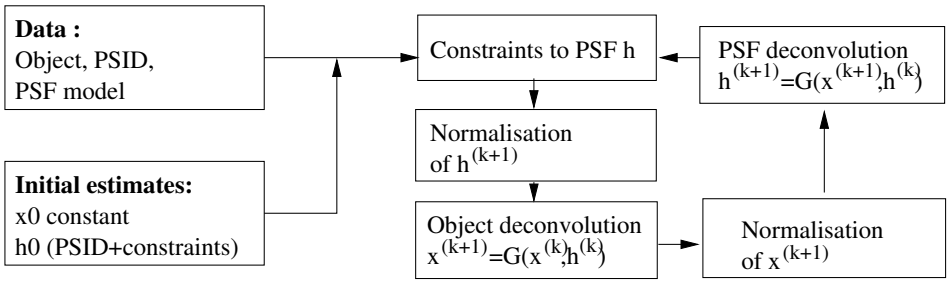


**Fig. 8.** Schematic representation of the iterative deconvolution algorithm. Both the unknown object and the hidden part of the PSF are reconstructed by the algorithm.

where $m_i$ is the sky background and $\epsilon$ a small value used to avoid a division by zero. After each iteration a constraint on the total intensity (due to the PSF normalisation) is applied to $\hat{x}_i^{(k+1)}$ to obtain the $(k+1)$ estimate $x_i^{(k+1)}$

The first test we performed made use of the complete PSF $h$ (inaccessible in real observations). It appeared that the results were far better than those obtained with the partially hidden PSID $B \times h$. Therefore we modified the algorithm to allow the reconstruction of the hidden part of the PSF as well as the object. This reconstruction was possible because strong constraints apply on the PSF, allowing its reconstruction using a Gerchberg-Saxton-Papoulis algorithm.

### Constraints on the PSF

The complete PSF of the convolution relation (eq. 2.8) is the interference function

$$I_0(\vec{r}) = \left| \sum_{k=1}^{N} \exp -\frac{2i\pi}{\lambda f}(\vec{r}.\vec{r}_k) \right|^2 \tag{3.4}$$

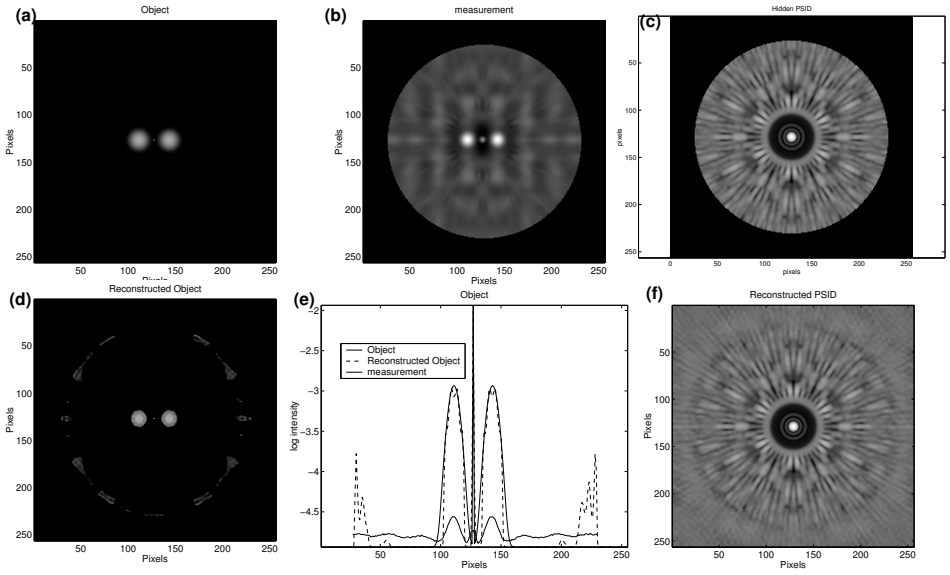


**Fig. 9.** Result of deconvolution for a 39 telescopes interferometer. (a): object; (b): observed blurred image with $N = 10^{10}$ photons ($N$ magnitude $\simeq 6$ for 1m telescopes and 20 s exposure time). (c): PSID (truncated PSF), supposed estimated on a close reference star. (d): result of the deconvolution of the object; (e) is a comparison of the object and the deconvolution result. (f) is the reconstructed PSF.

This function could in principle be computed analytically since the subaperture positions $\vec{r}_k$ in the output pupil are known. In practise instrumental and turbulence effects could affect the PSF; we decided indeed to use this analytic model as a first estimate. Three constraints were used in our algorithm:

1. Positivity
2. The PSF is known inside the boundaries of the enveloppe
3. The PSF has a calculable limited support in the Fourier plane. In monochromatic light, its Fourier transform is a finite sum of Dirac delta functions.

Fig. 7 shows a simulation of the PSF for the 39 telescope pupil of the example of Fig. 6 in polychomatic light ($\lambda = 10\mu$m, $\Delta\lambda = 2\mu$m). The central part of the PSF (in the middle), referenced in this paper as PSID, is known. Picture of the right is the Fourier transform of the PSF, showing a clearly limited circular support. This support is either calculated or estimated on the Fourier transform of the PSID (both supports are the same).

**The complete algorithm**

We propose an algorithmic structure based on the descent algorithm presented

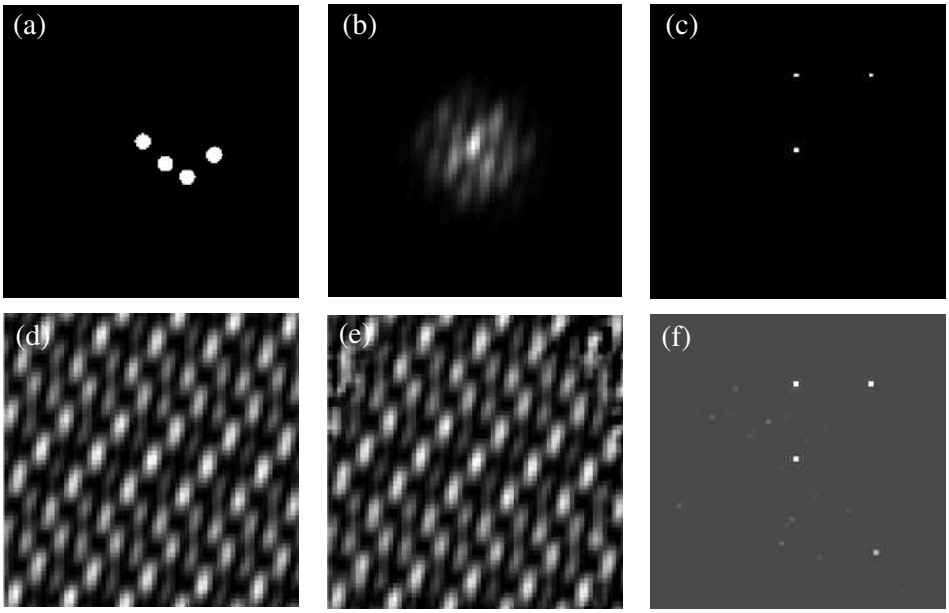


**Fig. 10.** Image reconstruction simulation for the VLTI/VIDA instrumental setup. (a): VLTI pupil. (b): interferometric image of the test object. (c): test object (triple star). (d): theoretical PSF. (e): Reconstructed PSF after 50 000 iterations. (f): Reconstructed object after 50 000 iterations.

above to reconstruct the object, as well as a Gerchberg-Saxton-Papoulis scheme to reconstruct the hidden part of the PSF. It is represented on figure 8, and is analogous to that proposed before (Lanteri et al., 1994, Ayers & Dainty, 1988) for blind deconvolution with, in our case a very strong constraint on the PSF.

Preliminary results are presented in fig. 9 for the 39 apertures hypertelescope already used for previous simulations. The test object is a centered Dirac delta impulse (point-source) surrounded by two symmetric gaussians. The intensity ratio between the central point-source and the gaussians is 10. The simulation is made at high-light level, number of photons in the estimated object and PSID is set to a value around $10^{10}$. The central wavelength is $10\mu$m and the bandwith is $2\mu$m.

The best reconstruction is attained after about 50 000 iterations. Smooth structures like the two gaussians are well reconstructed with a few iterations. The central point-source needs further processing. In the reconstructed object, the intensity ratio between the central Dirac and the gaussians is 8.8 (10 in the test object). We also notice the presence of a faint (intensity is 1.5% of the maximum) ghost ring at the cutoff location of the PSID. Further tests are currently being performed on the algorithm.

Another application to the deconvolution algorithm has been performed in the

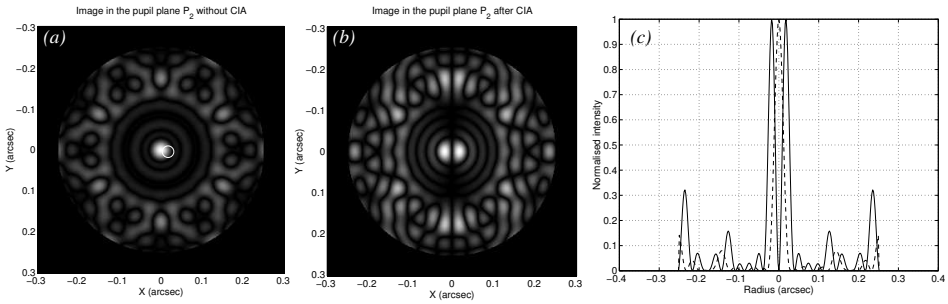


**Fig. 11.** Simulation of double stars monochromatic images ($\lambda = 10\mu$m) in the pupil plane with and without coronography. (a) gray-level plot of the intensity without AIC for a magnitude difference of 5 and a separation of 10 mas (1/3 of the intererometer resolution). The companion (not visible) is depicted by the white circle. (b) the same with AIC (the dynamic of the plot has been reajusted) (c) intensity profiles along the $x$-axis (solid line is with AIC, dotted line is without, maximum scaled to 1 for both curves).

particular case of VLTI/VIDA: the 4-pupil hypertelescope composed by the 4 UTs of the VLTI (Lardire et al., XXXX), using a single mode fiber beam combiner. In this case, the enveloppe of the fringe pattern is a Gaussian and the PSID has no longer a limited support. The algorithm has been adapted to that configuration and first results are shown on Fig. 10 for a test triple star object (zero magnitude difference between the stars) without photon noise. Pictures (e) and (f) show the reconstructed objet and PSF after 50 000 iterations.

## 4 Nulling

Detecting very faint companions around a star becomes an optical challenge with the increasing magnitude difference. For a ExPN such as 51 Pegb this difference is of the order of 7 in N-Band. Various coronographic techniques have been proposed (14 and references therein) to reject the energy of the on-axis star. The Achromatic Interfero Coronograph (AIC) 5 appears as particularly suitable for ExPN detection with the IRAN interferometric configuration. Total nulling of the light incoming from an on-axis source can be achieved if the complex amplitude is a pair function of space, i.e. for a symmetric telescopes configuration.

A numerical simulation has been performed in monochromatic light with a symmetric telescope configuration composed of 36 apertures spread over 3 rings (as in the previous section). We put 6 equally-spaced telescopes on the first ring, 12 on the second and 18 on the outer ring. The external diameter is 76 m, the wavelength is 10 $\mu$m. Corresponding image plane $P_1$ displays a set of 36 Airy discs with the same geometry: in particular the complex amplitude is a pair function. In that case, for a perfect wavefront the nulling effect is total.

Double star simulations are shown in Fig. 11 for two different separations be-

tween the components: a small separation of 10 mas (to be compared to the interferometer resolution of 30 mas) and a large separation of 200 mas where the companion falls inside the "dirty" zone of the main star's image. It can be seen that in both cases the secondary companion can be easily detected. Note that for this simulation the magnitude difference is chosen to be 5, but since the on axis star is fully nulled one would detect ExPNs for any magnitude difference for a perfect wavefront through the whole atmosphere and interferometer+AIC -coronagraph optics. Therefore technical set-up and atmospherical conditions will be the only limitation to our proposed nulling concept. A study of the AIC performances can be found in the litterature (Baudoz et al., 2000a, 2000b).

## 5 Discussion

The advantage of using a diluted array over a large monolithic mirror, assuming the primary telescopes were mobile across the interferometric array (like the VLA radio interferometer), is that the angular resolution of the interferometric array could be adaptively changed to match the angular separation of a star and its companion. A Fizeau-type is not however optimum in terms of sensitivity because the coherent energy dilutes among more and more fringes with expanding baselines. The alternative pairwise beam-combination is on the other hand inefficient when a very large number of sub-apertures were to be recombined. All-in-one combination of a large number of sub-pupils using IRAN approach is attractive because the coherent energy concentrates in almost one pixel. Since the convolution relation subsists across the output stacked pupils any extended object will produce a one-to-one image inside that pupil, also optimum in terms of read-out and background noise. The shortcoming of IRAN however is that for imaging applications only a small central "clean-field" can be straightforwardly used. Even in this case deconvolution techniques could be applied to get rid of side-lobe noise.

The fact that IRAN produces a pseudo-Airy pattern inside the output stacked pupil arises the problem of central obscuration of the secondary mirror in a classical Cassegrain-coudé set-up of the telescopes. Thus the central zone of IRAN's field of view is "blind" to the on axis component of the source which is imaged by the interferometer. Off-axis primary telescope mirror combinations would therefore be preferable to apply IRAN, a solution which is also desirable for thermal IR interferometry to minimize background optics emission.

## 6 Conclusion

We have presented a beam-combination technique with remarkable imaging properties for high dynamic imaging with diluted optical arrays. By construction the densified image and stacked-remapping technique from IRAN can be naturally combined with the Achromatic Interfero-Coronagraph (Gay & Rabbia, 1996), particularly suitable for coronographic imaging and detection of ExPNs compared to Labeyrie's densified pupil.

A number of questions remain open: the optimal beam combination, the effect of degrading co-phasing on the IRAN focal image, the formal definition of coronographic and/or nulling imaging of extended sources with IRAN. The fore-coming studies and results will hopefully contribute to select the best beam-combination of next generation imaging optical arrays like the VLTI or extension of already opertaing imaging arrays like NPOI. However such arrays have not been originally designed for densified imaging since their PSF exhibits strong secondary interference maxima due to their sparse and irregular input array configuration. It is therefore mandatory that future synthesis arrays with a large number of primary telescopes such as the proposed antarctic intererometer KEOPS (Vakili et al., 2004a, 2004b) involve an input baseline geometry which optimizes the PSID for its application to imaging/nulling schemes such as our proposed method.

## References

Aristidi E., Vakili F., Abe L., Belu A., Lopez B., Schutz A., Lanteri H., Menut J.L., 2004, SPIE conf on Astronomical BLABlA, Glasgow, June 2004

Ayers G.R., Dainty J.C., 1988, Opt. Let. 13, 547

Baudoz P., Rabbia Y., Gay J., 2000a, A&AS 141, 319

Baudoz P., Rabbia Y., Gay J., Burg R., Petro L., Bely P., Fleury B., Madec P.-Y., Charbonnier F., 2000b, A&AS 145, 341

Bracewell R. N., 1978, Nature 274, 780

Chelli A., Mariotti J.-M. 1986, A&A, 157, 372C

Gay J., Rabbia Y., 1996, C.R. Acad. Sci. Paris, 322 Série IIb, 265

Gillet, S., Riaud, P., Lardière O., Dejonghe J., Schmitt J., Arnold L., Boccaletti A., Horville D., Labeyrie, A., 2003, A&A 400, 393

Labeyrie A., 1996, A&A Suppl. 118, 517

Lantéri H., Aime C., Beaumont H., Gaucherel P., 1994, SPIE proc 2312, 182

Lantéri H., Roche M., Gaucherel P., Aime C., 2002, Signal Processing, 82, 1481

Lardière O., Schneider J., 2005, "'VIDA: A direct spectro-imager for the VLTI", ESO Astrophysics Symposia Proceedings, in press.

Mariotti J.-M., Coudé du Foresto V., Perrin G., Zhao P., Léna P., 1996, A&AS. 116, 381

Michelson A. A., 1920, ApJ 51, 257

Rousselet-Perraut K., Mourard D., Vakili F., 1997, Optical Engineering 36, 980

Soummer R., Aime C. Falloon P. E., 2003, A&A 397, 1161

Vakili, F., Aristidi, E., et al., SF2A-2003, Eds.: F. Combes, D. Barret and T. Contini. EdP-Sciences, Conference Series, p. 365.

Vakili, F., Aristidi, E., Abe L., Lopez B., 2004a, A&A, in press

Vakili, F., Aristidi, E., Fossat E., Abe L., Agabi A., Belu A., Lopez B., Domiciano A., 2004b, SPIE conf., Glasgow, June 2004